Resonance shifts in the multiphoton ionization of cesium atoms

J. Morellec, D. Normand, and G. Petite
Service de Physique Atomique, Centre d'Etudes Nucléaires de Saclay, BP No. 2-91190 Gif-sur-Yvette, France
(Received 15 December 1975)

This work reports the multiphoton ionization of cesium atoms, via resonance with the $6F$ level, by interaction with a single transverse and longitudinal mode neodymium-glass laser beam. At a low rate of ion production, when the laser frequency is tuned through resonance, the laser intensity necessary to create a constant number of ions passes through a minimum, as expected, for a three-photon energy equal to the unperturbed $6S \rightarrow 6F$ transition energy. But for a higher ionization rate, involving larger laser intensities, a departure from expectation is observed which is interpreted as a consequence of an energy shift of the transition. The level shifts are demonstrated in another way by their strong effect on the experimental order of nonlinearity of the interaction, K_{expt}. A sharp variation of K_{expt} is observed when the energy shift of the $6S \rightarrow 6F$ transition exactly compensates the wavelength detuning of the laser. The latter method gives shift values which are found to be independent of the large variations of the interaction volume under conditions of resonance. Both methods give a linear dependence of the shifts on the laser intensity. Identification of these shifts with energy shifts of the $6S \rightarrow 6F$ transition is subject to theoretical reservations and needs further experimentation.

I. INTRODUCTION

Many experiments on multiphoton ionization of gases or vapors have been reported in the past few years.[1-30] Most of them concerned interaction between atoms and the field of multimode lasers operating at fixed frequencies. The variation of the number of ions created in the interaction was generally investigated as a function of the laser intensity. The relatively large discrepancies observed between experimental results and theoretical calculations were mainly attributed to the poor coherence of the radiation and the possible contribution of quasiresonant states which enhance the ionization probability.

It has been recently demonstrated in this laboratory that laser coherence can greatly influence the multiphoton ionization processes[24,26]; we now consider it necessary to use a single-mode laser to eliminate variation in the observed ion yields owing to photon statistics. Such experimental measurements have been carried out; presently, a good understanding of multiphoton ionization processes depends mainly on an understanding of resonance phenomena.

The multiphoton ionization process becomes resonant when the energy of K_1 laser photons corresponds to the energy of an allowed transition to an intermediate atomic state. From the intermediate state to the continuum the atom must absorb another K_2 photons, $K_2 = K_0 - K_1$, where K_0 is the order of nonlinearity of the direct process; $K_0 = \langle W_i/h\nu + 1 \rangle$, where W_i is the ionization potential and ν is the frequency of the radiation. Generally, K_2 is much smaller than K_1, and the resonant process is governed by the first transition. It can be considered as a process of the K_1th order, and its probability is much larger than the probability of the direct process, which is of the K_0th order of nonlinearity. Resonance is therefore characterized by a large enhancement of the number of ions created in the interaction. The second characteristic lies in large variations of the experimental order of nonlinearity, which is the slope of the curves representing, in log-log coordinates, the number of ions, N_i, as a function of the laser intensity I,

$$K_{\text{expt}} = \frac{\partial \log N_i}{\partial \log I}. \tag{1}$$

K_{expt} has been found to be equal to K_0 when the laser was tuned to wavelength far from resonance, but significantly greater or smaller than K_0 when conditions of resonance were approached by variation of the laser wavelength.[21,23,27,28] In some experiments[28] the large variations of K_{expt} near resonance were explained as resulting from a shift of the resonant level. In a previous paper[21] we reported that the maximum of the ionization probability curve coincided with the position of the resonance wavelength. It thus seemed difficult to connect to the shift of the resonant level the K_{expt} variations, which extended over several tens of wave numbers. In all of these experiments, the large laser spectral bandwidth has been a great impediment to conclusive interpretation of the K_{expt} variations by means of level shift.

The purpose of this paper is to report an experimental study of four-photon ionization of cesium atoms via a resonant intermediate state, $6F$, by a single mode Q-switched neodymium glass laser beam.

The improvements relative to multimode radiation are typically a definite time-space distribution

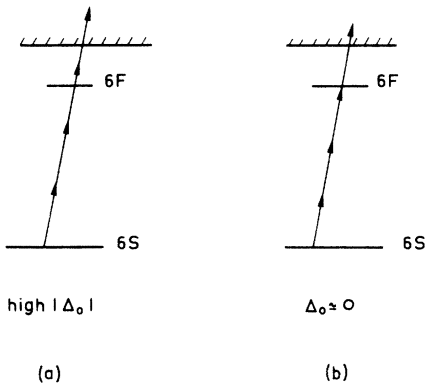

FIG. 1. Four-photon ionization of the cesium atom (a) by the direct process and (b) through a resonance on the $6F$ level. Δ_0 is the static detuning, $\Delta_0 = E_{6F} - E_{6S} - 3E_p$, where E_{6F} and E_{6S} are the energies of the $6F$ and $6S$ levels and E_p is the energy of one photon.

of the laser intensity and a narrow laser spectral linewidth of about 50MHz, which is of the same order of magnitude as the free-atom-level linewidth. Figure 1 summarizes the two processes competing in this experiment, (a) a process in which the atom in the $6S$ level absorbs four photons and is therefore directly ionized, and (b) a two-step process in which the cesium atom originally in the $6S$ state absorbs three photons to the resonant $6F$ level and is then ionized by a one-photon absorption.

II. THEORY

Multiphoton processes are conveniently handled by time-dependent perturbation theory. In the off-resonance case, using a theory developed from the evolution-operator formalism, the problem can be easily solved by considering the lowest-order non-vanishing term which is supposed to describe the phenomenon of interest.[1,2,5,31-34] In this case, for a given photon energy, the ionization probability depends on the laser intensity in the following way:

$$\mathcal{W} = \Gamma F^{K_0}, \tag{2}$$

where Γ is a coefficient depending on the atomic characteristics and on the field frequency, F is the photon flux, and K_0 is the minimum number of photons necessary to ionize the cesium atom.

Unfortunately, in the resonant case, i.e., when the energy of one or several photons approaches that of a transition line, it can be seen that higher-order terms which had been neglected in the evolution-operator expansion are no longer negligible. These higher-order effects have been taken into account by Gontier and Trahin[35] in a theory using the S-operator technique. They have shown that these higher-order terms arising from the S-operator expansion give rise to a shift and a broadening of the atomic levels. In the particular case where resonance occurs upon the absorption of $K_0 - 1$ photons, they derive an expression for the ionization cross section which, in our case, can be expressed as follows:

$$\sigma^{(K_0=4)}(\omega_p, F) = \frac{4\pi^2 r_0^2}{\alpha^3}\left(\frac{F}{F_0}\right)^3 \frac{1}{\omega_p}\rho(4\omega_p)\left|\sum_{i,j}\frac{\langle 6S|\vec{\epsilon}\cdot\vec{p}|i\rangle\langle i|\vec{\epsilon}\cdot\vec{p}|j\rangle\langle j|\vec{\epsilon}\cdot\vec{p}|6F\rangle\langle 6F|\vec{\epsilon}\cdot\vec{p}|f\rangle}{(\omega_{6S}+\omega_p-\omega_i+\Delta_i)(\omega_{6S}+2\omega_p-\omega_j+\Delta_j)(\omega_{6S}+3\omega_p-\omega_{6F}+\Delta_{6F})}\right|^2, \tag{3}$$

where r_0 is the Bohr radius, α the fine-structure constant, F the photon flux, F_0 $(=c/2\pi r_0^3)$ a reference flux, ω_p the field frequency, $\vec{\epsilon}$ the field polarization, $\vec{p}$ the electron momentum, $|f\rangle$ the final state, and $\rho(4\omega_p)$ the density of final atomic states. No account is taken of the structure of $6F$ and $6S$ levels. Furthermore, the summation runs over two complete sets of atomic states, $|i\rangle$ and $|j\rangle$, rather than three, since in the third step only the resonant process has been considered. The quantities Δ_i, Δ_j, and Δ_{6F} are expressed as follows:

$$\Delta_i = \frac{F}{F_0}\sum_k\left(\frac{\langle i|\vec{\epsilon}\cdot\vec{p}|k\rangle\langle k|\vec{\epsilon}\cdot\vec{p}|i\rangle}{(\omega_{6S}+\omega_p-\omega_k)+\omega_p)} + \frac{\langle i|\vec{\epsilon}\cdot\vec{p}|k\rangle\langle k|\vec{\epsilon}\cdot\vec{p}|i\rangle}{(\omega_{6S}+\omega_p-\omega_k)-\omega_p}\right), \tag{4a}$$

$$\Delta_j = \frac{F}{F_0}\sum_l\left(\frac{\langle j|\vec{\epsilon}\cdot\vec{p}|l\rangle\langle l|\vec{\epsilon}\cdot\vec{p}|j\rangle}{(\omega_{6S}+2\omega_p-\omega_l)+\omega_p} + \frac{\langle j|\vec{\epsilon}\cdot\vec{p}|l\rangle\langle l|\vec{\epsilon}\cdot\vec{p}|j\rangle}{(\omega_{6S}+2\omega_p-\omega_l)-\omega_p}\right), \tag{4b}$$

$$\Delta_{6F} = \frac{F}{F_0}\sum_m\left(\frac{\langle 6F|\vec{\epsilon}\cdot\vec{p}|m\rangle\langle m|\vec{\epsilon}\cdot\vec{p}|6F\rangle}{(\omega_{6S}+3\omega_p-\omega_m)+\omega_p} + \frac{\langle 6F|\vec{\epsilon}\cdot\vec{p}|m\rangle\langle m|\vec{\epsilon}\cdot\vec{p}|6F\rangle}{(\omega_{6S}+3\omega_p-\omega_m)+\omega_p}\right), \tag{4c}$$

where $|k\rangle$, $|l\rangle$, and $|m\rangle$ are three complete sets of atomic states.

In all of these formulas $\hbar = c = 1$ and we have neglected damping terms in the process. In the analysis of these formulas, we point out two different effects: Since Δ_{6F} is small compared to the energy

of the $6S \rightarrow 6F$ transition, when ω_p approaches $\omega_R = \frac{1}{3}(\omega_{6F} - \omega_{6S})$, the term $\omega_{6S} + 3\omega_p - \omega_{6F} + \Delta_{6F}$ in Eq. (3) becomes very small and the cross section very large. Exact resonance occurs when $3\omega_p$ matches the energy difference between the perturbed $6F$ level of energy $\omega_{6F} - \Delta_{6F}$ and the $6S$ ground state. Here, with no account being taken of the linewidths of either the atom or the field, the cross section becomes infinite.

Second, let us consider Δ_i, Δ_j, and Δ_{6F}. In the expression of Δ_j, the denominator of the first term in the large parentheses vanishes when resonance occurs on the $6F$ level, and Δ_j takes very large values, in contrast to Δ_i or Δ_{6F}. Then, if an atomic level is in the vicinity of the virtual state corresponding to the absorption of two photons, the expression $\omega_{6S} + 2\omega_p - \omega_j + \Delta_j$ may become zero, and an induced resonance may occur. This possibility is carefully analyzed in Ref. 35.

The formula (3), which is probably one of the more precise to describe multiphoton ionization processes, nevertheless contains some shortcomings. First, it does not exhibit any shift of the ground state, which must certainly appear in the case we are considering. Taking into account these effects involves some renormalization calculations which can be performed only in a more sophisticated treatment, which is now in progress.[36]

Second, no evaluation of Δ_j of Eq. (4b) is available for the case of cesium. Thus, although it is doubtful that in our case an induced resonance can occur, the role of these processes is not clear. They could possibly explain an important feature of the experimental data on resonant multiphoton ionization, which is the asymmetry of the cross-section curves.[21] There is also the interesting work of Feneuille and co-workers[37,38] on this subject. Using a formalism introduced by Fano[39] to treat the autoionization problem, they attribute this asymmetry to interference effects between resonant and nonresonant processes. The application of their method to our case has not yet been completed, but it seems rather promising.

The shift of the energy of the $6S \rightarrow 6F$ transition, due to coupling with the discrete spectrum, has been estimated and is found to be linear in the laser intensity, at least in the range considered in this paper ($\simeq 10^9$ W/cm^2). Thus it appears that within the limit of the approximations used here our experimental results must be mainly relevant to the frequency shift of the $6S \rightarrow 6F$ transition. Therefore a large part of this paper is devoted to its experimental measurement. Two different methods were employed. The first one is very similar to the classical method, which consists of measuring the shift of the maximum of the experimental resonance curve. The second one, proposed and already used by Bakos,[28] takes advantage of the effect of this resonance shift on the curves $\log N_i = f(\log I)$.

III. EXPERIMENTAL CONDITIONS

A. Laser beam

Figure 2 shows the experimental setup. The oscillator has already been described in a previous publication.[29] The laser beam is of a single transverse and longitudinal mode, Gaussian, and linearly polarized. Wavelength can be tuned from 10 560 to 10 600 Å by means of a birefringence filter inserted in the cavity. Transverse mode se-

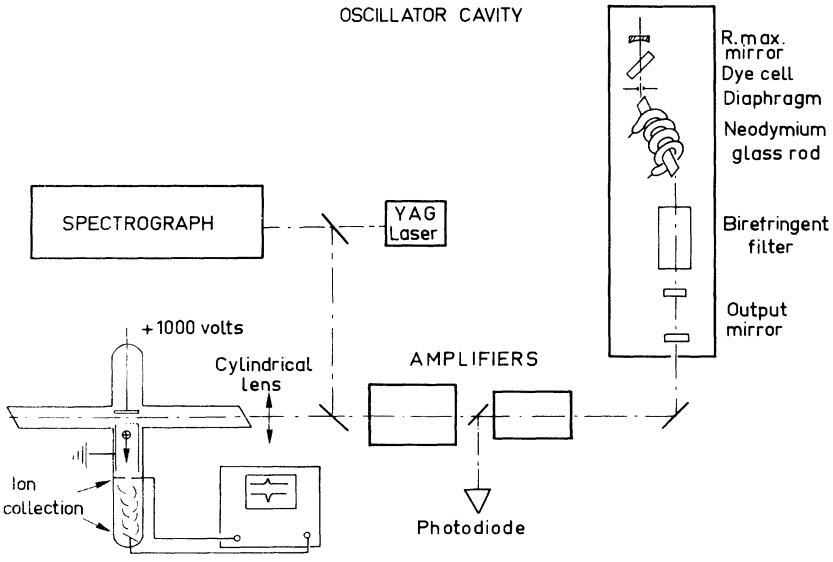

FIG. 2. Experimental apparatus.

lection is achieved by means of a circular diaphragm placed close to the back spherical mirror. Longitudinal mode selection is due to the combined action of the dye Q switching, the birefringence filter, and the output Fabry-Perot interferometer. Good single-mode operation is checked by a fast photodiode and a spectrograph. The pulse is of Gaussian shape and its duration is 37 nsec (full width at half-maximum).

B. Cesium atomic density

As reported previously,[30] the collected atomic ions are produced either by ionization of atoms or by a two-step ionization dissociation of cesium molecules. The two species of atomic ions, both originating in the interaction volume, cannot be separated by the time-of-flight spectrometer. As the molecular process involves the simultaneous absorption of only three photons, its probability is much higher than the ionization probability of atoms, and the laser intensities needed for the atomic process are large enough to saturate the molecular process. Then

$$N_i(Cs_2^+) = n_0(Cs_2)V_k, \tag{5}$$

where $n_0(Cs_2)$ is the density of molecules, V_k is the interaction volume for a kth order process, and $N_i(Cs_2^+)$ is the number of molecular ions created in the interaction.

The ratio R of molecular density $n_0(Cs_2)$ over atomic density $n_0(Cs)$ in the vapor strongly depends on the temperature of evaporation.[40] Therefore the atomic beam flowing from an oven heated to a temperature of[41] 152 °C has been replaced by cesium vapor in the saturated-vapor-pressure condition at a temperature of 25 °C. The ratio R in the atomic beam, assumed to be the same as that in the oven, was $R = 8 \times 10^{-4}$. In the new conditions, the atomic and molecular densities deduced from the vapor-pressure tables[40] are $n_0(Cs) = 6 \times 10^{10}$ and $n_0(Cs_2) = 1.1 \times 10^6$ cm^{-3}. The ratio R has been minimized by a factor of 40. In fact, the molecular process will be neglected in the experiment to be reported, which deals, furthermore, with a selectively resonant phenomenon for the cesium atoms.

C. Laser beam focusing and ion collection

The laser beam is focused by a planocylindrical lens of 350 mm focal length (Fig. 3). Because of the plane shape of the interaction volume, the ion flow moving through the field-free space of the time-of-flight spectrometer has a small divergence. The slit (1×10 mm) can be X or Z oriented and selects the ions created in a small region

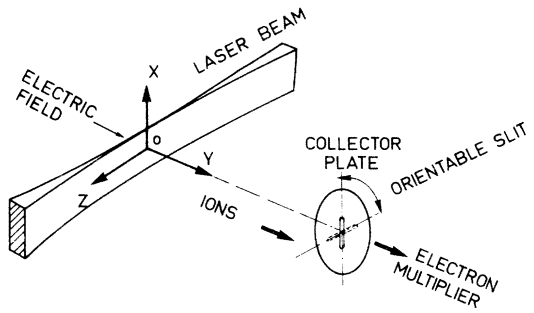

FIG. 3. Experimental arrangement, focusing and ion collection.

of the interelectrode space around the center 0. The good angular resolution of the system is demonstrated by comparing the ion signals on the collector and on the electron multiplier (Fig. 4). The dispersion in time on the Fig. 4(a) oscillogram corresponds, for the ions measured on the collector plate, to a dispersion in speed (in direction and in intensity), depending on the shape and size of the interaction volume. On the other hand, the small time duration of the electron multiplier signal means that the ions collected have the same speed and that they were created in the same region of the interelectrode space, and they were therefore accelerated by the same electric field. This good angular resolution will be very useful when measuring the effects on the interaction volume of the large variations of K_{expt} (see the Appendix).

D. Laser intensity

The laser energy is measured by a TRG thermopile and allows, as reported below (see the Appendix), the determination of the space-time distribution of the laser intensity by means of photometric measurements.

We can now define the different quantities to be considered in the experiment: N_{is} is the number of ions collected through the slit by the electron multiplier, N_{ip} the number of ions measured on the collector plate, and N_i the number of ions created when no discrimination on the method of collection is necessary. λ_L is the laser wavelength, and λ_R

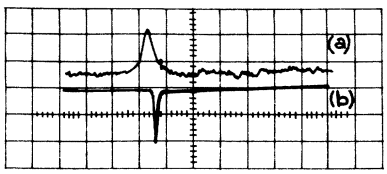

FIG. 4. Ion signals on (a) the collector plate and (b) the electron multiplier. Time scale: 2 μsec/cm.

is the 10 589.6-Å wavelength of resonance. Δ_0 is the $E_{6F} - E_{6S} - 3E_p$ static detuning, also called field-free detuning; δE is the energy shift of the transition $6S - 6F$; and $\Delta = \Delta_0 + \delta E$ is the dynamic detuning. I_M is the peak laser intensity, $\mathcal{E}_L$ the laser energy in a pulse, $K_0 = \langle W_i/h\nu + 1 \rangle$ the theoretical order of nonlinearity, and $K_{\text{expt}} = \partial \log N_i / \partial \log I$ is the experimental order of nonlinearity. K_{expt} is the slope of the curve representing the number of ions as a function of the laser intensity. n_0 is the neutral density, and V_k and τ_k are the interaction volume and interaction time, respectively, defined in detail in the Appendix.

IV. EXPERIMENTAL RESULTS

A. Ion-yield measurements

The experiment consists of measuring the number of ions as a function of the laser intensity, as represented in log-log coordinates in the diagrams of Fig. 5. The experiment is repeated over a number of laser wavelength values around resonance. The data shown cover the useful range of the detection system, where both linearity and a favorable signal-to-noise ratio prevail. As can be seen in Fig. 5, the curves are translated in the intensity

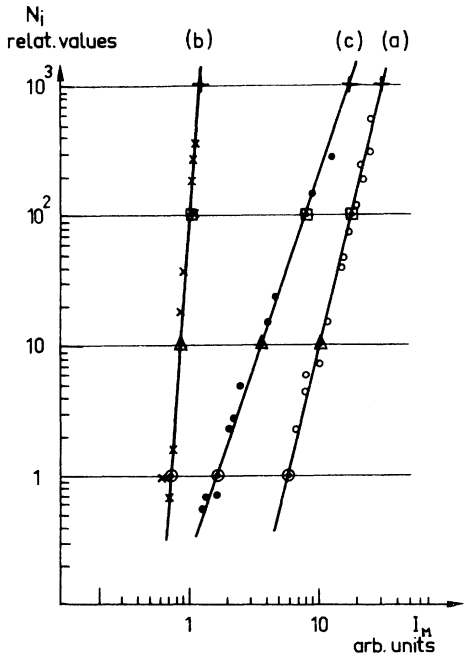

FIG. 5. Number of ions as a function of the laser intensity (relative values) for three different values of the laser wavelength ($\lambda_R = 10\,589.6$ Å). (a) $\lambda_L = 10\,558.1$ Å $< \lambda_R$; (b) $\lambda_L = 10\,588.9$ Å $< \lambda_R$; (c) $\lambda_L = 10\,590.85$ Å $> \lambda_R$. Intersections with horizontal lines for four values of N_i will be used to determine the lines of constant ion yield of Fig. 6.

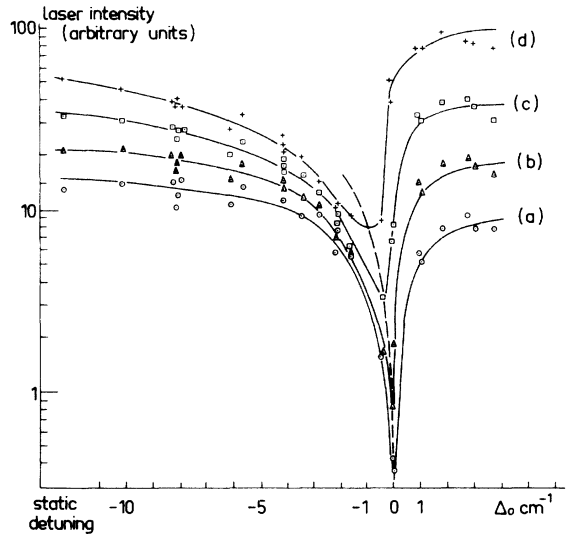

FIG. 6. Laser intensity vs static detuning for four values of the parameter N_i (number of ions); lines of constant ion yield. (a) $N_i = 1$, (b) $N_i = 10$, (c) $N_i = 10^2$, (d) $N_i = 10^3$ (relative values).

range and their slopes are considerably increased near resonance. Plotting the number of ions against the laser wavelength, the laser intensity being a parameter, would have then required extrapolations over orders of magnitude. We have therefore chosen to demonstrate resonance by the functional dependence upon the static detuning of the laser intensity necessary to create a constant number of ions (Fig. 6). The curves are lines of constant ion yield which exhibit minima when $\lambda_L \simeq \lambda_R$ and $\Delta_0 \simeq 0$.

Moreover, this representation is similar to the threshold-flux curves calculated in one theoretical paper.[1] These minima of laser intensity have the same meaning as the maxima of ionization probability. They are supposed to represent the exact resonance. The shifts of minima for rising values of the parameter N_i, as indicated by the dashed line in Fig. 6, are therefore considered as shifts of resonance, and, within some restrictions discussed further, give the correspondence between the laser intensity (absolute values) and the shift of resonance. These results will be compared in Fig. 10 with other shift values obtained by another method.

B. Interpretation of K_{expt} variations

Resonant ionization is not only characterized by an increase of the ionization probability but also by important variations of the experimental order of nonlinearity, K_{expt}, previously defined. In Fig. 7, K_{expt} is expressed as a function of the static

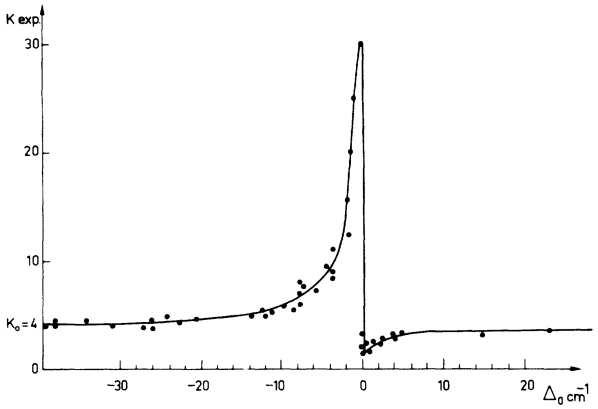

FIG. 7. Variation of K_{expt} as a function of the static detuning.

detuning. The diagram shows a slight increase of K_{expt} from the value of 4 for a static detuning $\Delta_0 = -40$ cm^{-1} to the value of 10 for $\Delta_0 = -4$ cm^{-1}. From there, K_{expt} rises increasingly rapidly up to 30 when $\Delta_0 = 0$. Then K_{expt} decreases sharply down to the value of 2; this phenomenon marks the resonance point. The curve then rises smoothly

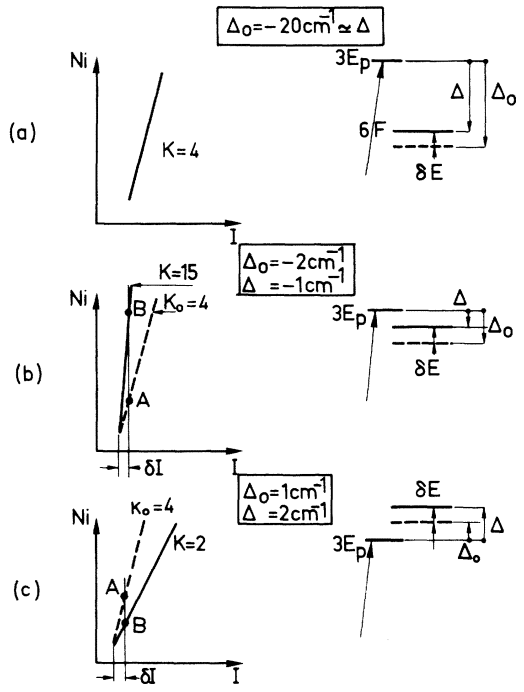

FIG. 8. Schematic representation of three typical situations demonstrating the strong effects of the level shifts on the experimental order of nonlinearity. (a) The static detuning Δ_0 is large and negative; $K_{expt} = 4$. (b) Δ_0 is negative and of the same order as the level shift; $K_{expt} = 15$. (c) Δ_0 is weak and positive; $K_{expt} = 2$. E_p is the photon energy, Δ is the dynamic detuning; $\delta E = 1$ cm^{-1} in the three cases.

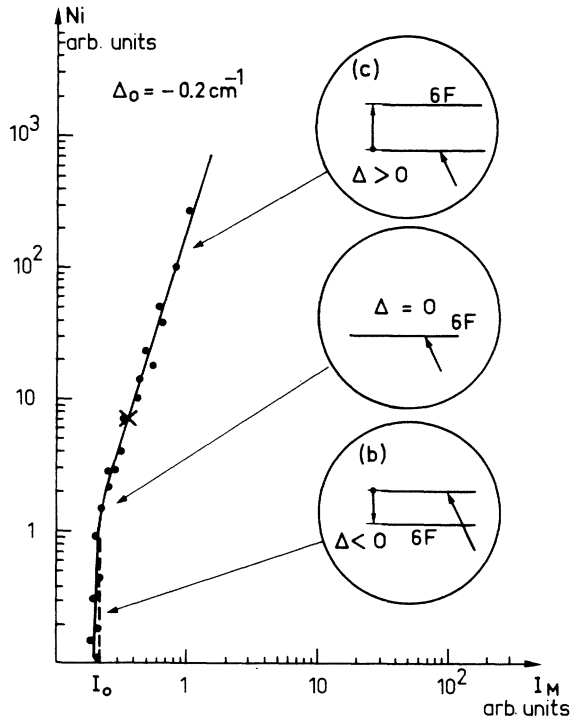

FIG. 9. Compensation of static detuning by level shifts. The upper part of the diagram refers to the case (c) in Fig. 8; the lower part corresponds to the case (b). The bend in the curve corresponds to the exact dynamic resonance $\Delta = \Delta_0 + \delta E = 0$, $\Delta_0 = -\delta E$. The cross denotes a situation described in space and time in Fig. 11.

toward the value of 4 for large positive detuning. We must observe that contrary to the multimode conditions previously reported[21] the present single-mode character of the radiation prevents the damping of resonance. Therefore resonance appears as a sharp phenomenon.

An interpretation of the K_{expt} variations is given in Fig. 8. In a small region of the atomic spectrum around the 6F level, the respective positions of the perturbed and unperturbed 6F levels, as well as the virtual state corresponding to the absorption of three photons, are shown. In each case the unperturbed level is denoted by the dashed line and the perturbed level by the solid line. Let us see in the three diagrams how the K_{expt} variations are governed by the level shifts:

(a) The static detuning Δ_0 is so large that the shift of the resonant level cannot affect the ionization probability which is then governed by the law I^{K_0}.

(b) The static detuning Δ_0 is negative and of the same order of magnitude as the level shift δE. An increase δI of the laser intensity produces a corresponding increase of δE which reduces Δ,

the dynamic detuning. The ionization probability rises not only because of the increased δI of the laser intensity but also because of the reduction by a factor of 2 of the detuning. Instead of assuming the value A on the line of slope K_0, the number of ions rises to a value B, which occurs on a straight line with a slope much greater than K_0.

(c) Now the static detuning is positive and therefore has the same sign as the level shift. This is the opposite of the previous situation and leads to a K_{expt} value smaller than K_0.

It must be noted that in this rough description the shift of only the $6F$ level has been considered. In fact, δE is the energy shift of the transition $6S \rightarrow 6F$.

C. Dynamic resonance study

The previous survey allows us to introduce the most interesting case, which is the exact compensation of the static detuning by the energy shift of the transition (Fig. 9). The lower part of the Figure is comparable to the (b) case of Fig. 8, where an increase of the laser intensity tends to achieve the exact resonance. The upper region is similar to the (c) picture, where an increase of the laser intensity raises the detuning from resonance. The transition between the two cases, respectively characterized by high and low values of the slope, is marked by the bend in the curve of Fig. 9, which therefore has the following features: $\Delta = 0$, and dynamic resonance is achieved; and $\delta E = -\Delta_0 = +0.2\ \text{cm}^{-1}$. I_0, the abscissa of the bend, is the laser intensity, which has shifted the energy of the $6S \rightarrow 6F$ transition by $0.2\ \text{cm}^{-1}$.

If the static detuning is increased, the laser intensity which allows the compensation is raised too, and the abscissa of the bend gives another pair of $(I_0, \delta E)$ values. The ion-yield measurements on the collector plate, less sensitive than electron-multiplier measurements, exhibit the same phenomenon, but for higher values of laser intensity and static detuning.

D. Resonance-shift measurements

The energy shifts of the $6S \rightarrow 6F$ transition, as measured by the dynamic compensation method, are compared in Fig. 10 to the shifts of the minima of the lines of constant ion yield (Table I). The laser intensity plotted in the abscissa is the peak laser intensity. The two curves show a variation of the energy shift linear in the laser intensity, but the dynamic compensation method gives a coefficient $\alpha = 4.3\ \text{cm}^{-1}/(\text{GW cm}^{-2})$, twice as high as the other method. The errors in the points of the dynamic compensation curve result from the uncertainties

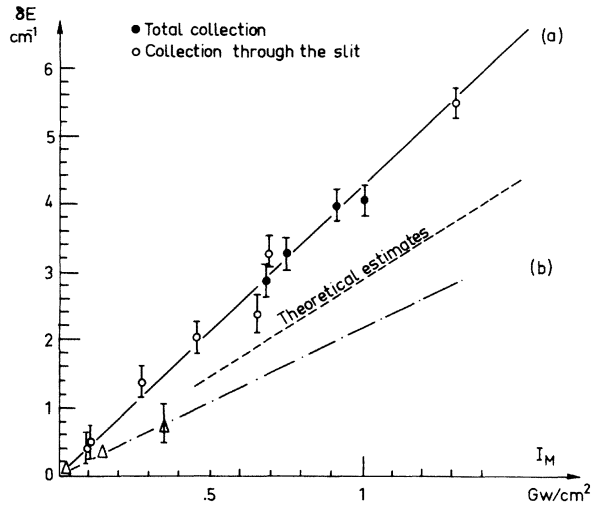

FIG. 10. Resonance shift vs the peak laser intensity. (a) Dynamic compensation measurements; (b) minima of lines of constant ion yield. The coefficients of linear dependence of δE on the laser intensity are $\alpha_a = 4.3$, $\alpha_b = 2.2\ \text{cm}^{-1}/(\text{GW cm}^{-2})$. Theoretical estimate: $2.9\ \text{cm}^{-1}/(\text{GW cm}^{-2})$.

in the laser wavelength $\delta\lambda_L = \pm 0.07$ Å. Larger uncertainties on the (b) curve are due to the broadening of the minima of the lines of constant ion yield for high values of laser intensity (see Fig. 6). Theoretical estimates show that level broadening does not have to be considered. Nevertheless, an intense laser field can remove the degeneracy of the levels involved here, and a small splitting may occur. As the components cannot be separated, this effect can only appear as a broadening which is too small, however, to explain the total widening of the lines of constant ion yield about their minima. Finally, both the broadening and the discrepancy between the two values of α given by the two methods of resonance-shift measurements lead one to suspect an effect arising from the interaction volume variations. This suggests a description, in time and space, of the ionization rate through conditions of dynamic resonance. For this purpose, a set of diagrams (Fig. 11) qualitatively

TABLE I. Shifts of minima of lines of constant ion yield for four values of the laser intensity.

Curve (Fig. 6)	λ_L (Å)	$3E_p$ (cm^{-1})	$\delta E_{6S \rightarrow 6F}$ (cm^{-1})	I ($10^9\ \text{W cm}^{-2}$)
a	10 589.60	28 329.68	~0	0.02
b	10 589.56	28 329.79	0.11	0.05
c	10 589.47	28 330.03	0.32	0.15
d	10 589.30	28 330.48	0.80	0.35

shows how the temporal and spatial distribution of the laser intensity acts on atoms in the interaction volume, taking into account the dynamic compensation of the static detuning.

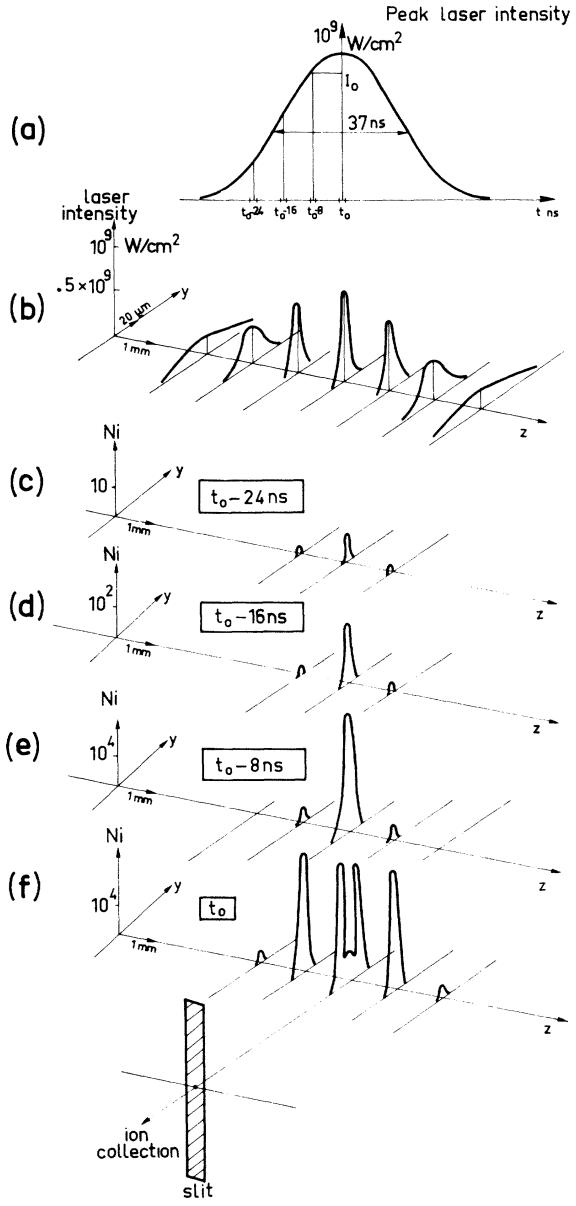

FIG. 11. Variation of the ionization rate as a function of time, in different sections of the interaction volume, taking into account the effects of level shifts. (a) Time distribution of the laser intensity for one laser shot; (b) spatial distribution at $t = t_0$ (maximum intensity). The four diagrams (c), (d), (e), and (f) represent at different times $t_0 - 24$ nsec, $t_0 - 16$ nsec, $t_0 - 8$ nsec, and t_0, the spatial distribution of the ions created during small time intervals dt. All of the spatial contributions are integrated over t and y by the slit represented at the bottom of the figure.

E. Space-time dependence of the ionization rate near resonance

Figure 11(a) represents the temporal distribution of the laser intensity, while 11(b) gives the spatial intensity distribution at $t = t_0$ along the y and z axes. The intensity is assumed to be roughly constant along the x axis, because of the cylindrical focusing (see Fig. 3). In Figs. 11(c), 11(d), 11(e) and 11(f), four instantaneous situations are distinguished, corresponding, respectively, to the times $t_0 - 24$ nsec, $t_0 - 16$ nsec, $t_0 - 8$ nsec, and t_0 refers to the time of maximum laser intensity. For each value of the parameter t, the number of ions created along the y and z axes during the time interval $(t, t + dt)$ is given in linear coordinates.

Fig. 11(c), $t = t_0 - 24$ *nsec*. The low value of the laser intensity allows us to neglect the level shift. The static detuning Δ_0 is the same over the entire interaction volume, $K_{expt} = K_0 = 4$.

Fig. 11(d), $t = t_0 - 16$ *nsec*. In the brightest spot of the interaction volume (for $z = 0$), the level shift $\delta E(I)$ is no longer negligible compared to the static detuning Δ_0; the slope is increased, $K_{expt} > K_0$. In the other xy planes, where the intensity is low, the level shifts are negligible and $K_{expt} = K_0$.

Fig. 11(e), $t = t_0 - 8$ *nsec*. A new increase of the laser intensity makes the level shift large enough, for $y = z = 0$, to exactly compensate for the static detuning; exact resonance conditions are locally achieved and a sharp dependence of the ionization probability on the laser intensity is obtained.

Fig. 11(f), $t = t_0$. The laser intensity is maximum. During the last 8 nsec, dynamic compensation has successively affected concentric zones increasingly distant from the center. When the laser intensity is higher than necessary for exact compensation, the $6F$ level is repelled out of resonance. This overcompensation regime is characterized by a large interaction volume and a low dependence of the number of ions on the laser intensity.

Since the depletion in atoms owing to the high ionization rate can be neglected, the second half of the interaction time leads to new contributions symmetric in space and time with those described above.

In our experiment, the collection slit has been chosen narrow enough to prevent any integration of the ions created along the z axis while the cylindrical focusing allows us to consider the laser intensity constant along the x axis. But the detector still integrates all of the y distributions during the whole interaction time. It must be noted that the description given in Fig. 11 typically corresponds to the cross in Fig. 9. When the laser intensity increases from I_0 to I_M, the number of

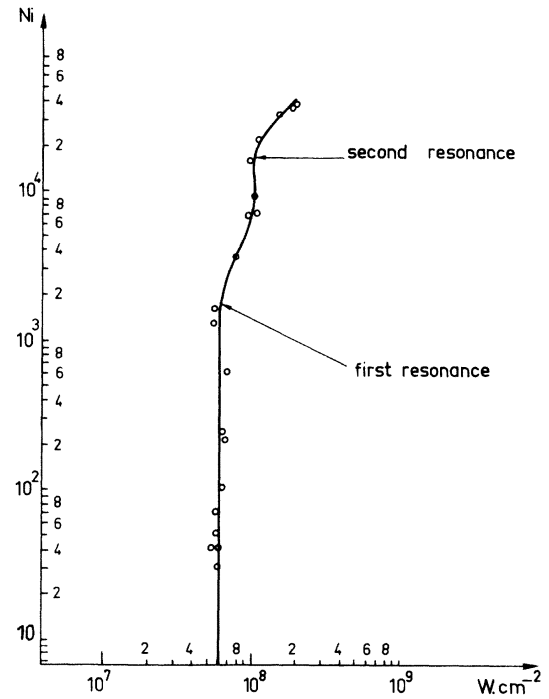

FIG. 12. Double resonance stemming either from the hyperfine structure of the ground level or from the doublet $6F_{5/2}$-$6F_{7/2}$.

ions created at the best focus, in a given time interval dt, decreases. Because of the summation on y and t, the collector slit detects only a slower rise in the dependence of N_i on I_M. The expansion and distortion of the interaction volume considerably complicates the relation between the number of ions collected and the laser intensity and can, at least qualitatively, explain the broadening of the minima in the lines of constant ion yield. In contrast, when dynamic resonance is achieved [Figs. 11(d), 11(e)] the ionization probability rises so sharply that the position of the bend in Fig. 9 is not significantly affected by the changes in the interaction volume.

F. Influence of the 6*S*- and 6*F*- level structure

Both ground and resonant levels have, in fact, an internal structure. The $6F$ is a doublet whose two sublevels $6\,^2F_{5/2}$ and $6\,^2F_{7/2}$ are separated by $0.1\,\mathrm{cm}^{-1}$. The $6S_{1/2}$ exhibits hyperfine structure[42] of $0.3\,\mathrm{cm}^{-1}$. In the case of cylindrical focusing, no experimental evidence has been given of the influence of these structures. This can be easily explained by the fact that the energy difference necessary to achieve the resonance on one or the other transition is of the order of 5 mJ, which is about our experimental error of energy measurements. The situation is different in the case of a collimated beam. There, the same absolute intensity difference in the interaction volume leads to an energy difference of several tens of mJ, which is easily detectable. Figure 12 shows a curve obtained with a collimated beam in the close vicinity of the resonance. It obviously exhibits two bends instead of the four expected. Their abscissas are separated by $4 \times 10^7\ \mathrm{W\,cm^{-2}}$. This intensity difference corresponds to a shift of $0.17\ \mathrm{cm}^{-1}$, which is of the order of magnitude of the level splitting involved here. Although the respective roles of the different sublevels involved here is not clear, we think that this particular result, which needs further investigation, must be attributed to the internal structure of 6S and $6F$ levels.

V. CONCLUSION

The resonant multiphoton ionization of cesium atoms by a single transverse and longitudinal mode laser has been investigated. The large variations of the experimental order of nonlinearity K_{expt} have been interpreted as stemming from shifts of resonance which strongly affect the ionization probability.

According to this interpretation, the break of K_{expt} from high to low values for rising laser intensities marks the achievement of the dynamic resonance, which is the exact compensation of the static detuning by the intensity dependent level shift. This particular feature of K_{expt} gives a correspondence between the shift of the resonance and the laser intensity which perturbs the atom. Shift values deduced from dynamic compensation measurements do not depend on the large interaction volume variations. In contrast, these variations significantly affect the number of ions measured under conditions of resonance.

The results obtained in this way lead us to make several remarks. Both methods give shifts linear in the laser intensity, and the agreement with the theoretical estimates seems rather good. This proves that no account need be taken of a resonant sixth-order shift owing to the three-photon coupling between 6S and $6F$ levels, at least in the intensity range we are working in. We point out that in this paper the energy shift of the $6S \rightarrow 6F$ transition has often been reduced to a shift of the $6F$ level. In fact, it results from the shifts of both 6S and $6F$ levels, which must be separated. Furthermore, an essential point is that all of these shift measurements are based on the assumption that the maximum of the ionization probability coincides with the exact resonant wavelength (taking into account the level shifts). We have seen in the theoretical survey that this is only an approximation. No experimental evidence of its validity has been

given yet, and the theoretical estimates are rather uncertain. Thus an ambiguity remains between the two usual acceptances of the word "resonance": wavelength at the maximum of ionization probability, or energy of the K_1 photons which matches an atomic transition energy. For all of these reasons, we are inclined to think that an accurate spectroscopic measurement of the real level shifts involved here will be necessary. This will allow separation of the $6S$ and $6F$ contributions to the energy shift of the transition. Moreover, agreement or disagreement of such spectroscopic measurements with our measured "resonance shifts" should be decisive in deciding the importance of other effects in these resonant ionization processes.

ACKNOWLEDGMENTS

The authors wish to express their gratitude to Dr. C. Manus and Dr. G. Mainfray for their direction and stimulating interest. We are indebted to Dr. Y. Gontier and Dr. M. Trahin for helpful discussions and to R. Laprade, D. Fondant, J. Delcher for technical assistance.

APPENDIX

From the formula (2), we can deduce the number of ions dN_i created in a small volume dv during the time dt.

$$dN_i = n_0 \Gamma I^k \, dv \, dt , \tag{6}$$

where n_0 is the neutral density and I is the local field intensity. In fact, the experimental number of ions is instead obtained as a function of the laser energy in a pulse, and the problem is to derive from this energy the field intensity or the photon flux, which are generally used in theoretical calculations. Moreover, if we want to obtain an experimental value of the ionization cross section from the total number of ions, we have to know the interaction volume, which, since the phenomenon is not linear, is different from the focal volume.

Focal volume

If z is the light-propagation direction, and if we neglect the field depletion owing to the ionization, we know that the energy $\mathcal{E}(z)$ which crosses any plane perpendicular to the z axis during a laser shot is conserved. Thus if $\mathcal{E}_L$ is the measured laser energy, we have

$$\mathcal{E}_L = \mathcal{E}(z) = \int I(x, y, z, t) \, dx \, dy \, dt , \tag{7}$$

where the integration is extended to the entire xy plane and to the pulse duration. In the case of a Gaussian pulse, after integration over t, we have

$$\mathcal{E}_L = \tau \int I(x, y, z) \, dx \, dy , \tag{8}$$

where τ is the $1/e^{\pi/4}$ width of the pulse. $I(x, y, z)$ can be expressed in the following form:

$$I(x, y, z) = I_M F(x, y, z) , \tag{9}$$

where I_M is the maximum intensity in the focal volume and $F(x, y, z)$ is a dimensionless shape factor. If the origin of coordinates is chosen at the point of best focus, we have

$$F(0, 0, 0) = 1 .$$

Thus we can write

$$\mathcal{E}_L = I_M \tau \int F(x, y, z) \, dx \, dy , \tag{10}$$

$$\mathcal{E}_L = I_M \tau S_z , \tag{11}$$

where S_z, which has the dimension of a surface, must not depend on z. Thus we have

$$I_M = \mathcal{E}_L / \tau S_z . \tag{12}$$

The value of S_z is obtained by photometric measurements. An infrared-sensitive photographic film is placed perpendicular to the z axis, and moved millimeter by millimeter on each side of the best focus. One photograph is taken in each position, the laser energy being kept constant. The photographs are then analyzed with an isodensitracer which draws the isophot lines representing the intensity distribution in the beam. Each area S_n included between two isophot lines corresponds to a small interval of optical density Δd centered around an optical density d_n. Taking account of the fact that F_n is normalized to unity at its maximum, F_n is known in every point of the focal volume, and S_z can be easily calculated as follows:

$$S_z = \left(\sum_n S_n F_n \right)_{(z)} , \tag{13}$$

and must be found constant for each value of z. The method, whose principle is summarized in Fig. 13, gives the following values:

$$S_0 = S_z = (0.38 \pm 0.04) \text{ mm}^2 .$$

In Fig. 14 the maximum value of F_n in each plane of constant z is plotted vs z. It represents the variation of the intensity along this axis.

Interaction volume

The total number of ions created in the interaction can be found via integration of Eq. (6) to be

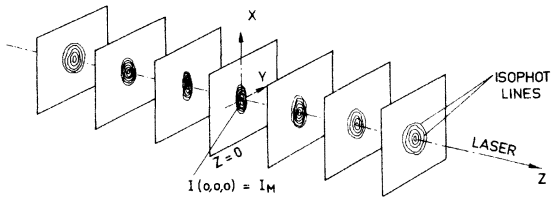

FIG. 13. Focal volume measurements. In a set of planes perpendicular to the laser axis, a photograph is taken and then analyzed by an isodensitracer. The intensity distribution is characterized by isophot lines.

$$N_{ip} = \Gamma n_0 \int I^k(x,y,z,t)\,dx\,dy\,dz\,dt\,, \tag{14}$$

if

$$I(x,y,z,t) = I_M F(x,y,z) G(t)\,. \tag{15}$$

Then

$$N_{ip} = \Gamma n_0 \tau_k I_M^k \int S_k(z)\,dz\,, \tag{16}$$

where

$$\tau_k = \int G^k(t)\,dt\,, \tag{17}$$

$$S_k(z) = \int F^k(x,y,z)\,dx\,dy\,. \tag{18}$$

$S_k(z)$ represents the contribution of a slice

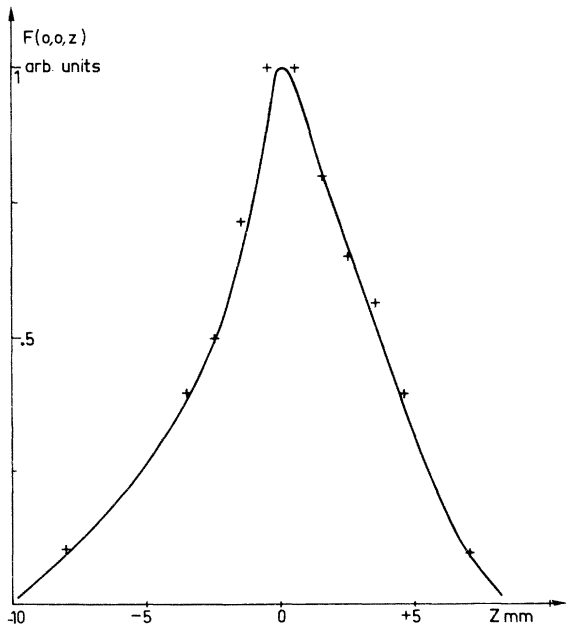

FIG. 14. Intensity distribution along the laser axis, normalized to unity, vs the distance to the best focus.

$(z, z+dz)$ to the ion creation. Contrary to S_z, it strongly depends on z and can be obtained from our photometric measurements as follows:

$$S_k(z) = \left(\sum_n F_n^k S_n\right)_{(z)}\,. \tag{19}$$

The interaction volume is

$$V_k = \int S_k(z)\,dz\,. \tag{20}$$

Since the effective order of nonlinearity, K_{expt}, can be very different from the off-resonance K_0 (equal to 4 in our case), it appears that the interaction volume must depend strongly on the laser wavelength, through the value of K_{expt}. This dependence is experimentally demonstrated in the following way: The laser is successively operated at three different wavelengths corresponding to three different values of Δ_0 (−20, −1, and +1 cm^{-1})

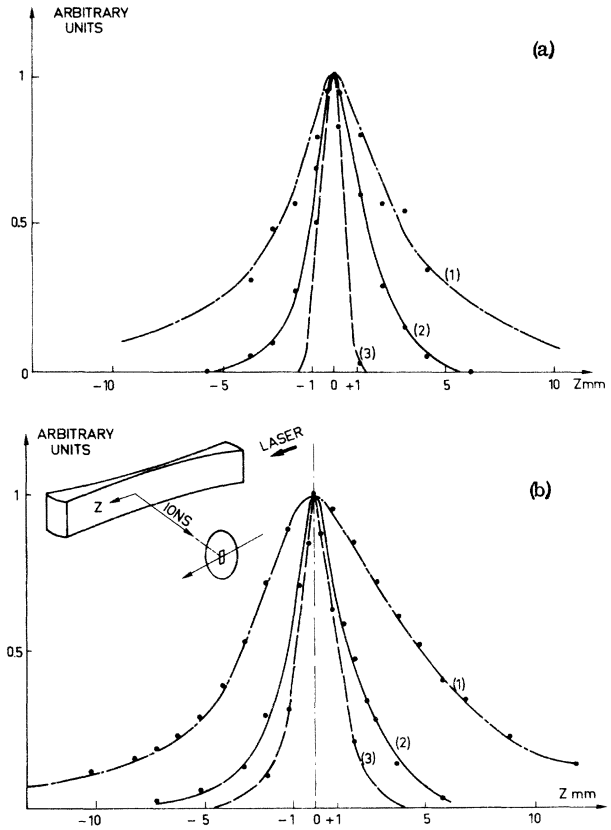

FIG. 15. Z distribution of the number of ions measured by two methods. (a) From photometric measurements, the contribution of each z = const plane to ion creation is calculated in three cases, (1) $k=2$, (2) $k=4$, (3) $k=15$. (b) Ion distribution is analyzed by moving the slit of the ion collector in front of the interaction volume for three values of K_{expt}. (1) $K_{\text{expt}}=2$, (2) $K_{\text{expt}}=4$, (3) $K_{\text{expt}}=15$. The three curves are normalized to unity.

and, respectively, to the three orders of nonlinearity, 4, 15, and 2. The ions created are collected by the electron multiplier through a 1-mm-wide slit which is moved in front of the lens focus from shot to shot, millimeter by millimeter, the laser energy being kept constant. The number of ions collected, N_{is}, must then be proportional to $S_k(z)\Delta z$, where Δ_z is the slit width.

Close to resonance, where we have seen that K_{expt} can depend strongly on the laser intensity, we have made sure that for the chosen value of the laser energy the exact resonance conditions are not achieved in any point of the interaction volume. Therefore K_{expt}, which is an average value on the whole interaction volume, can be accepted as representative of the phenomenon in this volume. In Fig. 15 the comparison of the two experimental dependences of $S_k(z)$ is made. Figure 15(a) shows the dependence of $S_k(z)$ on z, where $S_k(z)$ is calculated from the photometric measurements. Figure 15(b) shows this dependence derived from the ion measurements. The very good agreement between these two results demonstrates the dependence of the interaction volume on the experimental order of nonlinearity. Three values of V_k have been calculated, and we have found

$$V_4 = 0.36 \text{ mm}^3, \quad V_{15} = 0.05 \text{ mm}^3, \quad V_2 = 1.2 \text{ mm}^3.$$

This explains why we are reluctant to give a value of the ionization probability instead of a number of ions created. We insist on the fact that if the exact resonance occurs at any point the rather simple image we have given of the interaction volume becomes completely false (Fig. 11). In particular, K_{expt} is then a function of space and time coordinates; this must be taken into account to perform the integrations which lead to the expressions of the interaction time and interaction volume. The calculations become rapidly intractable, and have not been performed. Therefore we feel that great precautions must be taken in this case before identifying a number of ions to an ionization probability.

[1]H. B. Bebb and A. Gold, Phys. Rev. 143, 1 (1966).
[2]H. B. Bebb, Phys. Rev. 149, 25 (1966); 153, 23 (1967).
[3]G. S. Voronov and N. B. Delone Zh. Eksp. Teor. Fiz. 50, 78 (1966) [Sov. Phys.-JETP 23, 54 (1966).
[4]J. L. Hall, IEEE J. Quantum Electron. QE-2, 361 (1966).
[5]V. M. Morton, Proc. Phys. Soc. (Lond.) 92, 301 (1967).
[6]I. Popescu, C. Ghita, and N. Niculescu, Phys. Lett. 24A, 276 (1967).
[7]Y. Gontier, and M. Trahin, Phys. Rev. 172, 83 (1968).
[8]P. Agostini, G. Barjot, J. F. Bonnal, G. Mainfray, C. Manus, and J. Morellec, IEEE J. Quantum Electron. QE-14, 667 (1968).
[9]S. L. Chin, N. R. Isenor, and M. Young, Phys. Rev. 188, 7 (1969).
[10]P. Agostini, G. Barjot, G. Mainfray, C. Manus, and J. Thebault, IEEE J. Quantum Electron. QE-6, 782 (1970).
[11]R. A. Fox, R. M. Kogan, and E. J. Robinson, Phys. Rev. Lett. 26, 1416 (1971).
[12]G. Baravian, R. Benattar, J. Bretagne, G. Callede, J. L. Godart, and G. Sultan, Appl. Phys. Lett. 18, 387 (1971).
[13]B. Held, G. Mainfray, C. Manus, and J. Morellec, Phys. Lett. 35A, 257 (1971).
[14]B. A. Zon, N. L. Manakov, and L. P. Rapoport, Zh. Ekp. Teor. Fiz. 61, 968 (1971) [Sov. Phys.-JETP 34, 515 (1972)].
[15]P. Lambropoulos, Phys. Lett. 40A, 199 (1972).
[16]J. Bakos, A. Kiss, L. Szabo, and M. Tendler, Phys. Lett. 39A, 317 (1972).
[17]P. Agostini, P. Bensoussan, and J. C. Boulassier, Opt. Commun. 5, 293 (1972).
[18]R. Evans and P. Thoneman, Phys. Lett. 39A, 133 (1972).
[19]G. A. Delone, N. B. Delone, and G. K. Piskova, Zh. Eksp. Teor. Fiz. 62, 1272 (1972) [Sov. Phys.-JETP 35, 672 (1972)].
[20]M. Lu Van, G. Mainfray, C. Manus, and I. Tugov, Phys. Rev. A 7, 91 (1973).
[21]B. Held, G. Mainfray, C. Manus, J. Morellec, and F. Sanchez, Phys. Rev. Lett. 30, 423 (1973).
[22]G. Brincourt, R. Caccioli, and Ch. Millet, Opt. Commun. 7, 384 (1973).
[23]D. T. Alimov, N. K. Berez'hetskaya, G. A. Delone, and N. B. Delone, Zh. Eksp. Teor. Fiz. 64, 1178 (1973) [Sov. Phys.-JETP 37, 599 (1973)].
[24]C. Lecompte, G. Mainfray, C. Manus, and F. Sanchez, Phys. Rev. A 11, 1009 (1975).
[25]E. H. A. Granneman and M. J. Van der Wiel, J. Phys. B 8, 1617 (1975).
[26]F. Sanchez, Nuovo Cimento 11, 305 (1975).
[27]G. A. Delone and N. B. Delone, Zh. Eksp. Teor. Fiz. Pis'ma Red. 10, 413 (1969) [JETP Lett. 10, 265 (1969)].
[28]J. S. Bakos, Phys. Lett. 41A, 163 (1972).
[29]G. Petite, J. Appl. Phys. 46, 3462 (1975).
[30]B. Held, G. Mainfray, C. Manus, and J. Morellec, Phys. Rev. Lett. 28, 130 (1972).
[31]W. Zernik, Phys. Rev. 132, 320 (1963); 133, A117 (1964); 135, A51 (1964); 172, 420 (1968).
[32]B. A. Zon, N. L. Manakov, and L. P. Rapoport, Zh. Eksp. Teor. Fiz. 61, 968 (1971) [Sov. Phys.-JETP 34, 515 (1972)].
[33]Y. Gontier and M. Trahin, Phys. Rev. 172, 83 (1968); Phys. Rev. A 4, 1896 (1971).
[34]Y. Gontier and M. Trahin, Phys. Lett. 36A, 463 (1971).
[35]Y. Gontier and M. Trahin, Phys. Rev. A 7, 1899 (1973).
[36]Y. Gontier and M. Trahin, Phys. Lett. 54A, 341 (1975).
[37]S. Feneuille and L. Armstrong, Jr., J. Phys. (Paris)

36, L235 (1975).
[38]L. Armstrong, Jr., L. B. Beers, and S. Feneuille, Phys. Rev. A 12, 1903 (1975).
[39]U. Fano, Phys. Rev. 124, 1866 (1961).
[40]A. N. Nesmeyanov, *Vapor Pressure of the Chemical Elements* (Elsevier, Amsterdam, 1963).
[41]Conditions of the experiment described in Ref. 30.
[42]H. R. Kratz, Phys. Rev. 75, 1844 (1949).